Variational Method for Dense Systems*

V. R. Pandharipande† and H. A. Bethe
Laboratory of Nuclear Studies, Cornell University, Ithaca, New York 14850
(Received 21 December 1972)

The variational method for calculating energy of quantum fluids, and its applications to the Bose liquid ^{4}He, Fermi neutron gas, and liquid ^{3}He are discussed. The correlation functions are parametrized by their healing distance, and can depend on the states occupied by the correlated particles in the model wave function. They are calculated by constrained variation of the lowest-order contributions. The healing distance has a prescribed value in lowest-order calculations, whereas it is sufficiently large in hopefully exact energy calculations. The many-body cluster contributions in Bose fluids are summed with successive approximations of an integral equation due to van Leeuwen *et al.* A simple diagrammatic cluster expansion is presented for Fermi liquids, and its direct diagrams are summed with the integral equation. The contribution of exchange diagrams is shown to decrease rapidly with the number of exchanges, and their sums are truncated after the energy has converged to within a few percent.

I. INTRODUCTION

An equilibrium mixture of hyperons, interacting through two-body potentials is the simplest model of dense matter, and its region of validity has been discussed by Bethe.[1] In the nonrelativistic limit of this model, the many-body Schrödinger equation

$$\left(\sum_i \frac{-\hbar^2}{2m_i}\nabla_i^2 + \frac{1}{2}\sum_{i,j} v_{ij}\right)\Psi(1\cdots N) = E\Psi(1\cdots N) \tag{1.1}$$

should be solved for the variationally determined ground-state composition to calculate the zero-temperature energy as a function of density. The strong repulsive core in v_{ij} prohibits the use of simple perturbation theory. Brueckner theory has been used to calculate the energy of pure neutron matter up to $\rho = 0.5/\text{fm}^3$, beyond which lowest-order Brueckner calculations become both difficult and uncertain.[2]

Equation (1.1) can also be solved variationally with a sufficiently general trial wave function. For practical reasons the form of the trial wave function is, however, restricted to

$$\Psi(1\cdots N) = \prod_{i<j} f_{ij}\Phi(1\cdots N), \tag{1.2}$$

where Φ is a model fluid state wave function, and the correlation function f_{ij} is determined by minimizing the energy.

At typical maximum densities in neutron stars[3] the unit radius r_0,

$$\tfrac{4}{3}\pi r_0^3\rho = 1 \tag{1.3}$$

almost equals r_c, the radius of the repulsive core in n-n potential. In liquid ^{3}He and ^{4}He also the r_0 at equilibirum density is a few percent less than the He-He atomic potential core radius. The binding energies of both types of liquid helium, Fermi ^{3}He and Bose ^{4}He liquid are known, and have been extensively studied by variational methods with the wave function of Eq. (1.2).[4,5] These liquids form a suitable testing ground for many-body techniques used in hyperonic matter, and hence calculation of their energies is discussed in considerable detail. The He-He atomic potential core is very hard and has r^{-12} behavior at small r. It tends to induce much stronger correlations than the n-n soft-core potential with its r^{-2} to r^{-3} behavior.[1] Thus liquid He is probably too severe a test for the theoretical methods. As far as statistics go, since there are many distinguishable hyperons of similar mass, hyperonic matter can be anywhere in between a Fermi and a Bose system when its composition is heterogeneous.

Expectation values with wave functions (1.2) are generally expanded in cluster series. In the next section, we briefly review a method[6] in which the variation is constrained to enable energy calculations with only the two-body clusters. Subsequent sections describe hopefully exact energy calculations with unconstrained variation. The results from the two methods are compared in the last section to ascertain the former's region of validity.

II. CONSTRAINED VARIATION

The physical assumption here is that the contribution of farther neighbors of a particle i to the instantaneous potential $\sum_j v_{ij}$ seen by i should mostly be included in the average field of which φ_i is an eigenfunction. Hence distant neighbors

should not be strongly correlated, and the effect of their correlation on the energy should be small. If this effect is neglected, one could in principle work with correlation functions satisfying the condition

$$\text{if } f_{ij} \neq 1, \quad \text{then all } f_{ik} = 1 \tag{2.1}$$

when ij are nearest neighbors. But it would be very difficult to handle Eq. (2.1) because $f(r_{ij})$ would depend on whether some other particle k is closer to i or j than r_{ij}, and thus the different f_{ij} would be coupled in a complicated way. In practice,[6] Eq. (2.1) is approximated as a healing constraint on a single f_{ij} as a function of r_{ij} as follows:

$$f_{ij}(|r_{ij}|>d)=1,$$
$$\frac{df_{ij}}{dr_{ij}}(|r_{ij}|=d)=0. \tag{2.2}$$

The healing distance d is chosen such that on the average there is only one particle within a distance d of an average particle. With this constraint correlations are at times allowed between second and more distant neighbors, while at times even the first neighbors are treated as uncorrelated. We hope that these effects cancel.

All direct contributions of many-body clusters are zero if Eq. (2.1) is valid, and we will show that many-body exchange diagrams, which can contribute even when Eq. (2.1) is valid, are small. Thus the energy can be calculated with only the two-body term in the cluster expansion, which is

$$\frac{E}{N}=\tfrac{1}{2}\rho\int\left(v-\frac{\hbar^2}{m}\frac{\nabla^2 f}{f}\right)f^2 d^3r \tag{2.3}$$

for Bose fluids. Before minimizing E with respect to variations in f, the part of v that contributes to the average field and hence does not induce correlations, must be subtracted from integral (2.3). In accord with constraint (2.2), we assume that the $v(r)$ for $r>d$ contributes *only* to the average field, so that the integral (2.3) now has the upper limit $r=d$. For $r<d$ the simplest (and quite reasonable) assumption is that a constant λ_0 is the contribution to the average field. This λ_0 is to be determined from constraint (2.2). Thus the variational equation becomes

$$\delta\int_0^d\left(-\frac{\hbar^2}{m}f\nabla^2 f+vf^2-\lambda_0 f^2\right)d^3r=0 \tag{2.4}$$

and gives directly the two-body "Schrödinger" equation for $r<d$

$$-\frac{\hbar^2}{m}\nabla^2 f+vf=\lambda_0 f. \tag{2.5}$$

The λ_0 can be obtained from the boundary condition (2.2), and is a function of d, which is determined from

$$\rho\int_0^d f^2 d^3r=1, \tag{2.6}$$

where the left-hand side is simply the average number of particles within d as calculated in lowest order. Equations (2.5) and (2.6) are solved simultaneously.

In Fermi fluids let us first consider pairs of distinguishable fermions like those of spin-up and spin-down particles of a given baryon type or of two different baryons of any spin direction. Such pairs are not exchanged in the antisymmetrization of the wave function. If the two particles are in states k_i and k_j, the two-body cluster contribution of their interaction is given by

$$(W+W_F)_{ij}=\frac{1}{\Omega}\int\varphi_{ij}{}^2 f^{ij\,2}\times\left[v-\frac{\hbar^2}{m}\left(\frac{\nabla^2 f^{ij}}{f^{ij}}+2\frac{\nabla f^{ij}\cdot\nabla\varphi_{ij}}{f^{ij}\varphi_{ij}}\right)\right]d^3r, \tag{2.7}$$

where f^{ij} is the correlation function for particles in model states $\vec{k}_i$, $\vec{k}_j$, and φ_{ij} is the relative wave function $e^{i(\vec{k}_i-\vec{k}_j)\cdot\frac{1}{2}\vec{r}}$. Since

$$\frac{\nabla^2\varphi_{ij}}{\varphi_{ij}}=-[\tfrac{1}{2}(\vec{k}_i-\vec{k}_j)]^2\equiv -k^2, \tag{2.8}$$

we can write Eq. (2.7) as

$$(W+W_F)_{ij}=\frac{1}{\Omega}\int\Psi^*\left(v-\frac{\hbar^2}{m}k^2-\frac{\hbar^2}{m}\nabla^2\right)\Psi d^3r, \tag{2.9}$$

with

$$\Psi=f^{ij}\varphi_{ij}, \tag{2.10}$$

and the constraint (2.2) as

$$\frac{\nabla\Psi}{\Psi}(\vec{r},\ |r|=d)=\frac{\nabla\varphi_{ij}}{\varphi_{ij}}(\vec{r},\ |r|=d). \tag{2.11}$$

It is convenient to decompose φ_{ij} and Ψ in partial waves

$$\varphi_{ij}(r)=\sum_{l,m} j_l(kr)P_l^m(\theta,\varphi)$$
$$\Psi(\vec{r})=\sum_{l,m} u_l(r)P_l^m(\theta,\varphi)/kr. \tag{2.12}$$

If v is spherically symmetric the various l states are not coupled, and the contribution of each can be minimized separately following the procedure described for the Bose fluids. The equation for u_l is obtained as

$$-\frac{\hbar^2}{m}\frac{d^2u_l}{dr^2}+\frac{\hbar^2}{m}\frac{l(l+1)}{r^2}u_l+vu_l=\left(\frac{\hbar^2}{m}k^2+\lambda_0^l\right)u_l \tag{2.13}$$

and λ_0^l is determined from the boundary condition

$$\frac{1}{u_l(d)}\frac{du_l(d)}{dr}=\frac{1}{j_l(kd)}\frac{d\,j_l(kd)}{dr}\,. \tag{2.14}$$

The correlation function f depends upon both k and l and may be written as

$$f_{ij}=\sum_l f^l(k,r)P_{ij}^l\,, \tag{2.15}$$

where the projection operators P_{ij}^l operate only on the model wave function by definition.

The same procedure can be followed in calculating the contribution of interaction between parallel-spin fermions of the same type in states $\vec{k}_i$ and $\vec{k}_j$. Adding the exchange contribution to Eq. (2.9) gives

$$(W+W_f)_{ij\uparrow\uparrow}=\frac{1}{\Omega}\int[\Psi^*(\vec{r})-\Psi(-\vec{r})]\times\left(v-\frac{\hbar^2}{m}k^2-\frac{\hbar^2}{m}\nabla^2\right)\Psi(\vec{r})d^3r\,, \tag{2.16}$$

and on substituting the partial wave expansion (2.12) in Eq. (2.16) the even l state contributions cancel, and those of odd states are doubled. The variational calculation of f_{ij} is unaffected because Eq. (2.13) is obtained by individually minimizing the contribution of each partial wave. The d is given by

$$\frac{1}{\Omega^2 N}\sum_{ij}\langle\varphi_i\varphi_j-\varphi_j\varphi_i\delta_{\uparrow\uparrow}\,|[\sum_l f^{l2}(\vec{k},\vec{r})P^l]\bar{O}(d)\,|\,\varphi_i\varphi_j\rangle=1\,, \tag{2.17}$$

where $\bar{O}(d)=1$ for $|r|<d$ and zero otherwise. Equations (2.12), (2.14), and (2.17) are solved simultaneously by iteration.

The above method is simple enough to study complex systems like dense hyperonic matter, and still sufficiently general to treat the small differences in baryon-baryon interactions, interactions in different angular momentum states, and baryon masses. It is also possible to generalize it to treat noncentral forces, particularly the strong tensor forces in neutron-proton interaction.[7,8]

However, there are approximations in this model justified by purely physical arguments. Particularly the healing distance d is obtained from a lowest-order calculation of the number of particles within d. This may not be valid when $d\gg r_0$ [the unit radius $r_0(1.3)$ equals d in uncorrelated systems]. In neutron star matter $d\sim 1.2r_0$, whereas in liquid helium $d\sim 1.4r_0$, because helium atomic cores are much harder than the baryonic cores. Secondly, the variational property $E\geq$ true E_0 is lost because the variational integrals are only evaluated in lowest order.

In subsequent sections, we describe hopefully exact calculations of E with sufficiently large values of d so that the effects of the constraint are negligible. In principle these are variational calculations with correlation functions given by solutions of Eqs. (2.5) and (2.13), and with the healing distance d considered a parameter.

The state dependence of the correlation function, and that of the potential in case of neutron matter, makes exact many-body cluster calculations in Fermi fluids very complex. However, we note that the short-range part of the neutron-neutron potential, which is mainly responsible for the correlations, is similar for all states. The coefficients of the n-n potential

$$v^l(r)=\sum_j a_{lj}\frac{e^{-j\mu r}}{\mu r} \tag{2.18}$$

are given in Table I for the Reid,[9] and the modified Reid potential of Bethe and Johnson.[1] The core strengths differ by only ~3% in various states of the modified Reid potential.

The l and k dependence of f as calculated from

TABLE I. The coefficients a_{lj} of n-n potentials, Eq. (2.18).

l \ j	1	2	4	6	7
0	−10.463	0	−1650.6	0	6484.2
Even > 0	−10.463	−12.322	−1112.6	0	6484.2
Odd (Modified)	3.488	3.01	−702.0	0	6699.0
Odd (Reid)	3.488	0	−933.48	4152.1	0

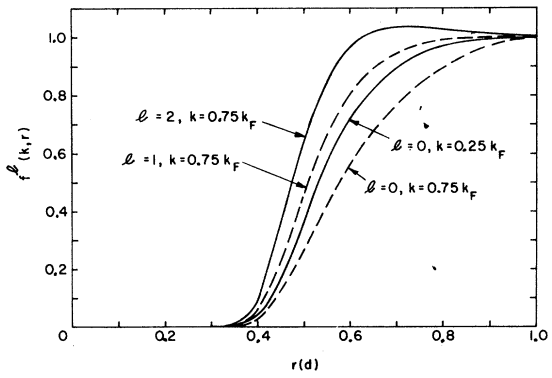

FIG. 1. The k and l dependence of f in liquid ^{3}He at $\rho=0.277$ Atoms/σ^3 and $d=2r_0$ with LJ potential.

Eq. (2.13) is also not too strong as shown in Fig. 1 for liquid ^{3}He and Fig. 2 for neutron matter. The correlation functions in these figures are calculated at $d = 2r_0$, and it will be shown in subsequent sections that the energy is insensitive to d when $d \gtrsim 2r_0$. The densities are 0.277 A/σ^3 (σ = 2.55 Å) and 2.4 n/fm^3. At these densities, the $r_0 \simeq r_c$ in both cases, and hence Figs. 1 and 2 are in some sense qualitatively comparable. The f in neutron gas is smoother than that in liquid He because the soft-core nature of the n-n potential allows the f to penetrate considerably inside the core. The rather sharp rise in the ^{3}He f may be attributed to the strong attraction in He-He atomic potential.

Only the $\varphi^* f \nabla f \cdot \nabla \varphi$ term in Eq. (2.7) is responsible for the state dependence of f in liquid ^{3}He, whereas the differences between the $v_l(r)$ also contribute to this dependence in neutron gas. The term is repulsive in relative s states ($l = 0$) and attractive when $l \geq 1$. It pulls the f_l's for large l inwards, and also makes the effective interaction more attractive as l increases.

If the $\varphi^* f \nabla f \nabla \varphi$ term is neglected, the resultant f for ^{3}He corresponds to that in a mass-3 Bose fluid. The angle average of this term is zero and consequently the average f^2 of the present calculations,

$$f_{\mathrm{av}}^2 = \frac{1}{N^2} \sum_{ij} (f^{ij})^2, \tag{2.19}$$

is very close to the f^2 of a mass-3 Bose fluid. The $f_{\mathrm{av}}{}^2$ in ^{3}He, neutron gas, and $f_{\mathrm{Bose}}{}^2$ in fictitious ^{3}He Bose fluid are compared in Fig. 3.

We note that the differences between various $f^l(k, r)$ are not too large. In subsequent sections, the calculation of many-body (>2) cluster contributions is considerably simplified by using a single $f_{\mathrm{av}}{}^2$.

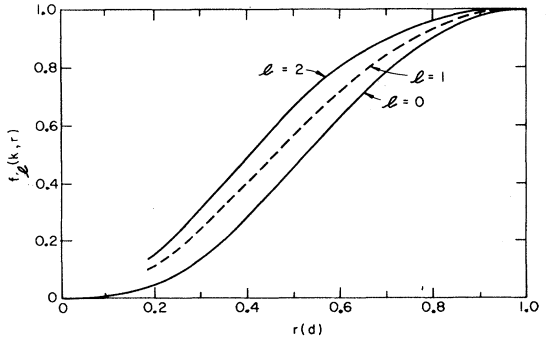

FIG. 2. The l dependence of f in n gas at 2.4 n/fm^3, $d = 2r_0$, $k = 0.55 k_F$, with the Reid potential.

III. CLUSTER EXPANSION OF RADIAL DISTRIBUTION FUNCTION

The radial distribution function of a Bose fluid is defined as

$$g_{mn} = \Omega \int \prod_{i<j} f_{ij}{}^2 d\tau' \Big/ \int \prod_{i<j} f_{ij}{}^2 d\tau, \tag{3.1}$$

where $d\tau'$ omits integration over r_{mn}, and Ω is the normalization volume. The subscripts denote coordinate variables of the functions; thus $g_{mn} = g(\vec{r}_{mn})$.

By convention, we antisymmetrize only the left-hand side Ψ^* in calculations of expectation values for Fermi fluids. Thus initially the particles 1, 2, ..., i, respectively, occupy plane-wave states $\varphi_1, \varphi_2, \ldots, \varphi_i$ with momenta $\vec{k}_1, \vec{k}_2, \ldots, \vec{k}_i$, and summation over particles is changed to summation over states. The radial distribution function for particles initially in states $\vec{k}_m$ and $\vec{k}_n$ can now be defined as

$$g(\vec{k}_m, \vec{k}_n) = \frac{\Omega \int (A \prod_i \varphi^*_{q,i})(\prod_{i<j} f_{ij}{}^2)(\prod_i \varphi_{i,i}) d\tau'}{\int (A \prod_i \varphi^*_{q,i})(\prod_{i<j} f_{ij}{}^2)(\prod_i \varphi_{i,i}) d\tau}, \tag{3.2}$$

where A is the antisymmetrizing operator, $\varphi_{q,i}$ is the abbreviation of $\varphi_q(\vec{r}_i)$, and all $f_{ij} = f_{\mathrm{av}}$. The true g is obviously

$$g(r) = \frac{2}{N(N-1)} \sum_{i<j} g(\vec{k}_i, \vec{k}_j). \tag{3.3}$$

The f_{ij} approaches unity at large r_{ij} and is small or zero at $r = 0$. It is then convenient to substitute

$$f_{ij}{}^2 = 1 + F_{ij} \tag{3.4}$$

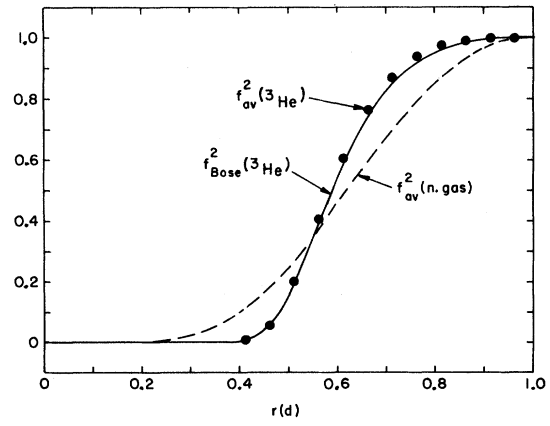

FIG. 3. The points, full, and broken lines, respectively, show the average f^2 in Fermi ^{3}He, f^2 in mass-3 Bose He, and average f^2 in n gas. See captions of Figs. 1 and 2 for details of densities, d, and potentials.

for all pairs other than mn in Eq. (3.1) or Eq. (3.2). The F_{ij} is a short-range function with absolute value generally less than unity, and products of $(1+F_{ij})$ can be expanded in powers of F as follows:

$$\prod_{i<j}(1+F_{ij}) = 1 + \sum_{i<j} F_{ij} + \sum_{i<j,k<l(ij\neq kl)} F_{ij}F_{kl} \cdots . \tag{3.5}$$

Integrals over various terms in Eq. (3.5) are represented by diagrams of the type shown in Figs. 4–6.

The points in these diagrams represent the particle coordinates, broken lines represent F functions, and numerator diagrams must always contain points m and n with $f_{mn}{}^2$. In Fermi fluid diagrams the full line $\vec{k}_q$ entering $\vec{r}_i$ represents the final state φ_q occupied by the particle i in the left-hand side Ψ^*. The lines $\vec{k}_1 \cdots \vec{k}_i$ must originate from points $1 \cdots i$, respectively, by our convention.

Diagrams of type C.2, C.4, and D.1 in which the state lines k_i originate and end in the same point are direct diagrams analogous to the Bose fluid diagrams A.2, A.4, and B.1, respectively. The small circles k_i in these diagrams simply contribute a unit factor. A line k_i going from i to j gives a factor $e^{i\vec{k}_i\cdot\vec{r}_{ij}}$, and the sign of a Fermi fluid diagram is given by $(-1)^{l+s}$, where l is the number of closed loops and s is the number of state lines. Diagrams of the type C.6 in which an uncorrelated particle is exchanged give zero contribution. Such

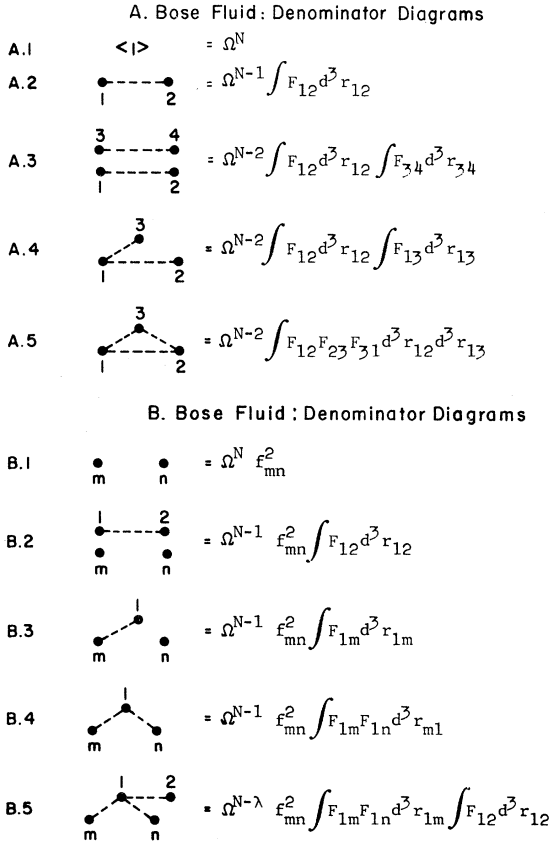

FIG. 4. Bose fluid diagrams.

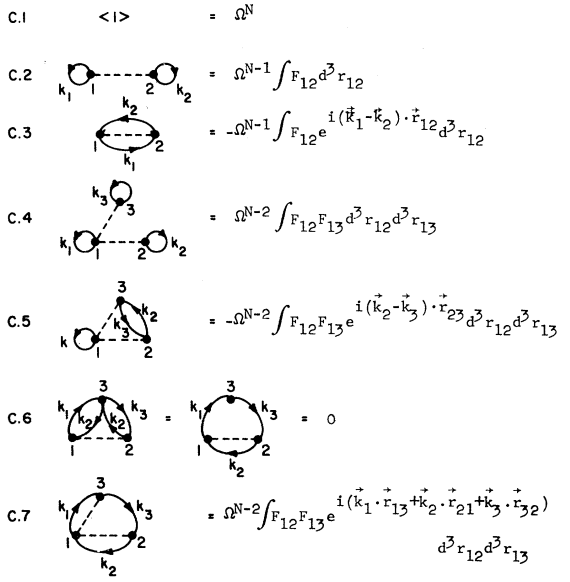

FIG. 5. Fermi fluid denominator diagrams.

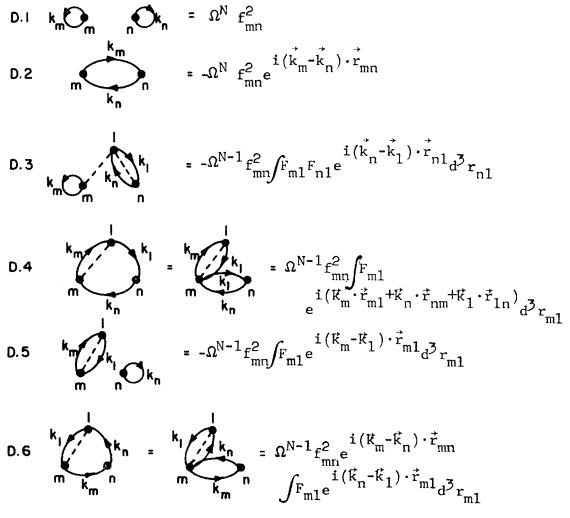

FIG. 6. Fermi fluid numerator diagrams.

diagrams contain an integral

$$\int e^{i(\vec{k}_i-\vec{k}_j)\cdot\vec{r}}d^3r$$

which is zero from orthogonality of φ_i's.

The contribution of diagrams like B.2, which contain two or more disconnected pieces, is simply the product of contributions from each piece (B.1 and A.2 are the disconnected pieces of B.2), apart from powers of Ω. The connected numerator diagrams of type B.3 or B.5 in Fig. 4, and D.5 or D.6 in Fig. 6, which can be broken into two separate parts at a single point are called factorable because their contribution appears as a product of two disconnected pieces. The connected nonfactorable diagrams of type B.1, B.4 in Fig. 1, and D.1, D.2, and D.3 in Fig. 3 are called irreducible. The diagram D.4 will be discussed subsequently.

If all disconnected and factorable numerator diagrams which contain a particular irreducible diagram are collected together, and the irreducible part is factored out, then its coefficient cancels the denominator within terms of order $(1/N)$. Thus g_{mn} is simply the sum of all irreducible diagrams divided by Ω^N.

Figure 7 illustrates this cancellation for the first two terms of the denominator in Bose fluids,

$$\text{Denominator} = \Omega^N\left[1+\frac{1}{\Omega}\tfrac{1}{2}N(N-1)\int F_{12}d^3r_{12}+\cdots\right]. \tag{3.6}$$

The irreducible diagram B.4 of Fig. 4 is considered for illustration. It is trivial to obtain the first unit term of Eq. (3.6) in the coefficient of B.4 in the numerator. The four diagrams that contribute to the second term of the coefficient are shown in curly brackets of Fig. 7. The first three are factorable and contribute

$$\frac{1}{\Omega}3(N-3)\int F_{12}d^3r_{12}.$$

Note that a factor Ω^N is taken out of these contributions to cancel the Ω^N in Eq. (3.6). The fourth disconnected diagram gives

$$\frac{1}{\Omega}\tfrac{1}{2}(N-3)(N-4)\int F_{12}d^3r_{12},$$

and the second term in the coefficient of B.4 in numerator becomes

$$\frac{1}{\Omega}\tfrac{1}{2}N(N-1)\int F_{12}d^3r_{12}-\frac{3}{\Omega}\int F_{12}d^3r_{12}.$$

The first part of above equals the second term of denominator (3.6) whereas the second part vanishes as $1/N$.

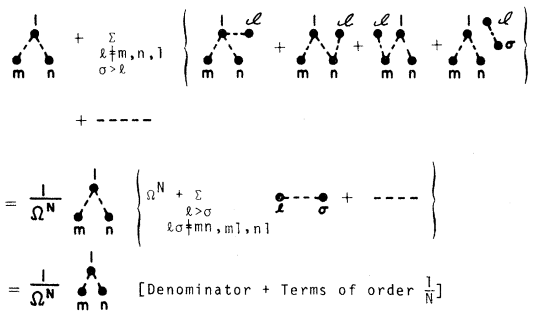

FIG. 7. Cancellation of denominator in Bose fluids.

The Fermi fluid numerator diagrams D.4 and D.6 appear to be similar and factorable. However, if D.4 is factored, the factor with f_{mn}^2 is

$$f_{mn}^2 e^{i(\vec{k}_1-\vec{k}_n)\cdot\vec{r}_{mn}},$$

which is the contribution of a diagram in which line k_1 originates from point m. Such a diagram is not allowed because in our convention the line k_i must originate from point i. Hence D.4 must be considered as a new irreducible diagram. The diagram D.2 is a factor of D.6, and its coefficient is simply one of the denominator diagrams C.3. Thus D.6 must be factored along with other factorable diagrams with D.2 as a common factor to cancel the denominator within terms of order $1/N$.

The diagrammatic method and the van Kampen cluster expansion[10] are identical in Fermi fluids up to at least three-body clusters, and probably more. The calculation of many-body clusters is, however, very laborious by the van Kampen method, and the main advantage of the above method is its simplicity.

Recently Gaudin, Gillespie, and Ripka[11] have attempted to cancel the denominator by collecting all diagrams containing a connected diagram. Thus their expectation values are sums of all connected (but not necessarily irreducible) diagrams. The denominator contains $N(N-1)/2$ diagrams of type C.2, whereas the number of numerator diagrams with D.1 and C.2 as unconnected parts is only $(N-2)(N-3)/2$. The leading term of the difference,

$$2N\Omega^{N-1}\int F_{12}d^3r_{12}/\Omega^N = 2\rho\int F_{12}d^3r_{12} \tag{3.7}$$

is clearly nonzero even when $N\to\infty$ and hence the denominator cannot be cancelled against only unconnected diagrams. Factorization of the $(2N-4)$ connected diagrams with D.1 and C.2 as factors essentially provides the difference [Eq. (3.7)].

IV. INTEGRAL EQUATION FOR SUMMING DIRECT DIAGRAMS

Some of the diagrams that contribute to the radial distribution function in a Bose system are shown in Fig. 8. A sum over all particles labeled by numbers 1, 2, ... is implied, and it simply gives a ρ with factors to account for double counting (for example, diagram E.7 gets a factor $\frac{1}{2}$). Thus the contribution of diagram E.2 is

$$f_{mn}{}^2\rho \int F_{1m}F_{1n}d^3r_1 \equiv f_{mn}{}^2 S_{mn} . \tag{4.1}$$

The functions F and S are shown in Fig. 9 for a typical f with $d = 2r_0$, in liquid ^{4}He near equilibrium density. Since the magnitude of S is larger than that of F, and they are of opposite sign, the contribution of diagram E.3,

$$f_{mn}{}^2\rho \int F_{1m}S_{1n}d^3r_1 \tag{4.2}$$

is larger than that of E.2. It can be easily seen

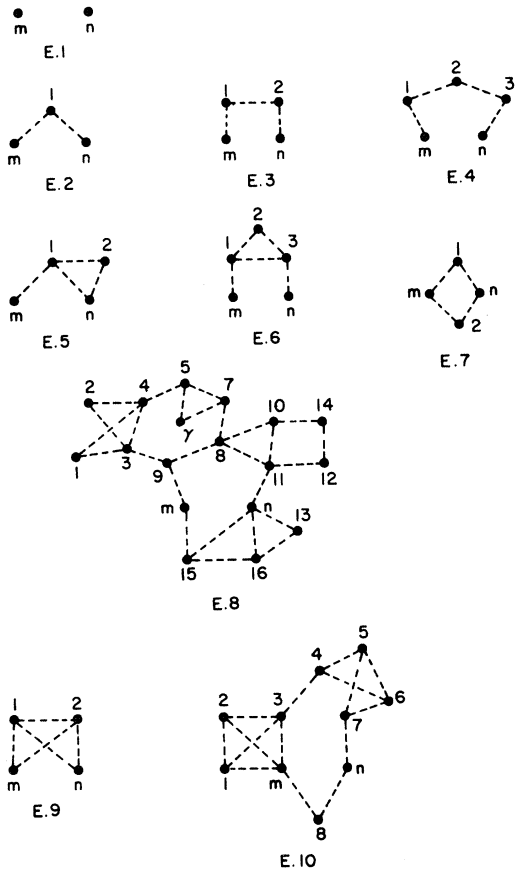

FIG. 8. Some irreducible diagrams that contribute to Bose $g(r)$.

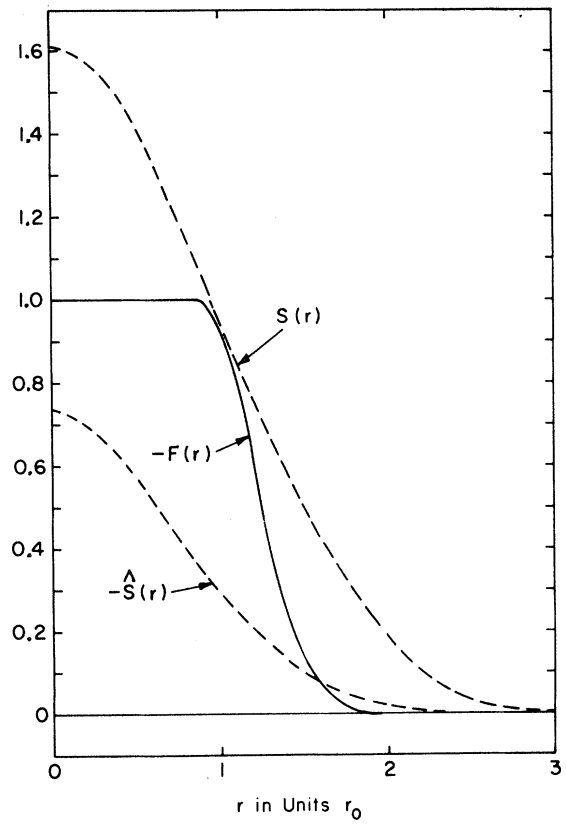

FIG. 9. The functions F, S, and $\hat{S}$ in liquid ^{4}He at $\rho = 0.35$ Atoms/σ^3, and $d = 2r_0$ with Lennard-Jones potential.

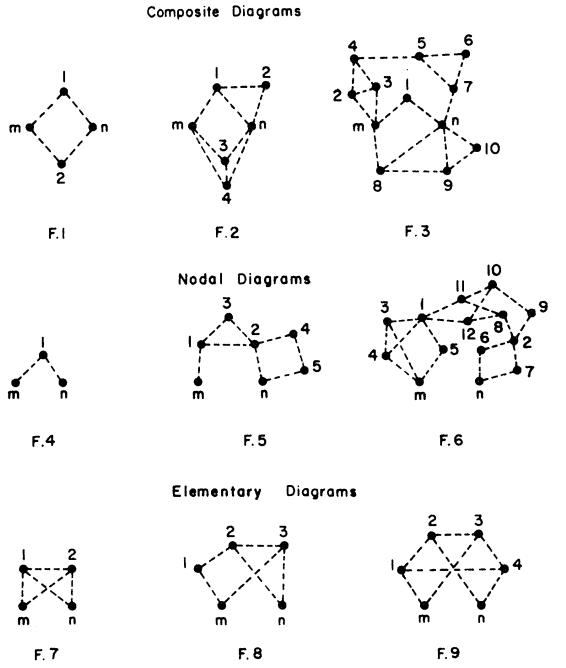

FIG. 10. Classification of Bose fluid diagrams.

that E.4 contributes more than E.3, etc. The diagrams E.2, E.3, ... are called single chains, and in dense fluids their contribution does not decrease with the number of particles in the chain.

The contribution of diagram E.5 is equal to

$$f_{mn}{}^2\rho\int F_{m1}F_{n1}S_{n1}d^3r_1, \tag{4.3}$$

is of the same order as that of E.2 because $S\gtrsim 1$ in the range of F. Thus diagrams of type E.5–E.7 in which additional chains are added to connect two particles in a chain are also of the order as those of single chains. Diagrams in which any two points of a chain may be connected by many chains are called hypernetted chains, and E.8 is a typical HNC diagram. No two chains or subchains are connected by an F.

The simplest diagram in which two chains connecting m and n are connected by an F is E.9. Its contribution $\hat{S}$ is small (Fig. 9), particularly in the region where $f_{mn}{}^2$ is appreciable, because all four particles have to be within the range of F. One would thus expect contributions of diagrams like E.10 involving E.9 as a subdiagram to be small.

All g_{mn} diagrams can be classified as composite, nodal, and elementary, as shown in Fig. 10. Composite diagrams have more than one unconnected path connecting m and n. In nodal diagrams, all paths connecting m and n must pass through at least one point. In diagrams F.4–F.6 the nodes are at points 1 and 2. All diagrams which are neither nodal nor composite are elementary. All HNC diagrams are either nodal or composite.

TABLE II. The radial distribution function for liquid ^{4}He at $\rho=0.35$ Atoms/σ^3, $d=2r_0$, with Lennard-Jones potential, in the lowest order, HNC, and HNC/4 approximations.

r (Å)	$g_{\text{L.O.}}$	g_{HNC}	$g_{\text{HNC/4}}$
1.406	0.7095×10^{-16}	0.6257×10^{-15}	0.5006×10^{-15}
1.856	0.1376×10^{-3}	0.7321×10^{-3}	0.6307×10^{-3}
2.306	0.7026×10^{-1}	0.2334	0.2183
2.756	0.4308	0.9521	0.9128
3.206	0.7809	1.242	1.228
3.656	0.9460	1.180	1.186
4.106	0.9943	1.057	1.068
4.556	1.0	0.9775	0.9857
5.006	1.0	0.9573	0.9593
5.456	1.0	0.9731	0.9703
5.906	1.0	0.9957	0.9919
6.356	1.0	1.008	1.006
6.806	1.0	1.009	1.009

The integral equation

$$-\ln\left(\frac{g_{mn}}{f_{mn}{}^2e^{E_{mn}}}\right)=\rho\int\left[g_{m1}-1-\ln\left(\frac{g_{m1}}{f_{m1}{}^2e^{E_{m1}}}\right)\right](g_{n1}-1)d^3r_1 \tag{4.4}$$

derived by van Leeuwen, Groeneveld, and de Boer[12] sums all composite and nodal diagrams formed from elementary diagrams included in E_{mn} and F. In the approximation $E_{mn}=0$, we get the familiar HNC equation[13]

$$\ln\left(\frac{g_{mn}}{f_{mn}{}^2}\right)=\rho\int\left[g_{m1}-1-\ln\left(\frac{g_{m1}}{f_{m1}{}^2}\right)\right](g_{n1}-1)d^3r_1 \tag{4.5}$$

whose consistent solution is the sum of all HNC diagrams. The next approximation, $E_{mn}=\hat{S}_{mn}$ gives the sum of HNC diagrams plus the elementary diagram F.7 and all HNC's in which F.7 substitutes or adds to a link. We call this approximation HNC/4.

Table II shows g_{mn} in lowest order, HNC, and HNC/4 approximations. There is little difference between HNC and HNC/4 distribution function when $g>0.1$, whereas $g_{\text{L.O.}}$ is a poor approximation except when r is large. Hence HNC/4 should be a fair approximation because addition of more complicated elementary diagrams involving more than four particles should produce changes smaller than the difference between HNC and HNC/4.

V. BOSE FLUID CALCULATIONS

Traditionally the kinetic energy part of the total energy E,

$$E=\int\left(\prod_{i<j}f_{ij}\right)\left(\sum_i-\frac{\hbar^2}{2m}\nabla_i{}^2+\tfrac{1}{2}\sum_{i,j}v_{ij}\right)\left(\prod_{i<j}f_{ij}\right)\Big/\int\prod_{i<j}f_{ij}{}^2 \tag{5.1}$$

is transformed using the Jackson-Feenberg[14] identity,

$$\int\Psi'^*\nabla^2\Psi d^3r=\tfrac{1}{4}\int\left[\Psi'^*\nabla^2\Psi+(\nabla^2\Psi'^*)\Psi-2(\nabla\Psi'^*)\cdot(\nabla\Psi)\right]d^3r \tag{5.2}$$

with

$$\Psi_i = \prod_{i<j} f_{ij} . \tag{5.3}$$

The $(\nabla_i f_{ij} \nabla_i f_{ik})$ terms cancel, and the entire kinetic energy can be included in an effective potential V_{JF},

$$V_{JF} = v_{ij} - \frac{\hbar^2}{2m}\left(\frac{\nabla^2 f_{ij}}{f_{ij}} - \frac{(\nabla_i f_{ij})^2}{f_{ij}^2}\right) \tag{5.4}$$

and

$$E_{JF} = \frac{1}{2\Omega}\sum_{ij}\int V_{JF}\, g\, d^3r . \tag{5.5}$$

We use E_{JF} to denote the energy as calculated above, and we have $E = E_{JF}$ when the true $g(r)$ is used in integral (5.5). When f satisfies Eq. (2.5) for $r<d$ then

$$V_{JF}(r<d) = \tfrac{1}{2}\left(v + \lambda_0 + \frac{\hbar^2}{m}\frac{(\nabla f)^2}{f^2}\right), \qquad r<d$$

and

$$V_{JF}(r>d) = v . \tag{5.6}$$

Alternatively the potential and the part of kinetic energy obtained by collecting terms in which ∇^2 operates on a single f can be included in an effective potential V, and "potential energy" W defined as

$$V = v - \frac{\hbar^2}{m}\frac{\nabla^2 f_{ij}}{f_{ij}}, \tag{5.7}$$

and

$$W = \frac{1}{2\Omega}\sum_{ij}\int V g\, d^3r . \tag{5.8}$$

This effective potential V is simply λ_0 for $r<d$ when f satisfies Eq. (2.5), and it is v when $r>d$. The ∇_i^2 operating on f_{ij} and f_{ik} gives additional kinetic energy U,

$$U = -\frac{\hbar^2}{2m}\frac{1}{\Omega^2}\sum_{ijk} g_3(\vec{r}_{ij}, \vec{r}_{ik})\frac{\nabla_i f_{ij}\cdot\nabla_i f_{ik}}{f_{ij} f_{ik}}\, d^3r_{ij}\, d^3r_{ik} , \tag{5.9}$$

where $g_3(\vec{r}_{ij}, \vec{r}_{ik})$ is a three-particle distribution function defined analogous to the radial distribution function g. The total energy of the Bose fluid is simply

$$E = W + U . \tag{5.10}$$

We use the superposition approximation[13]

$$g_3(\vec{r}_{ij}, \vec{r}_{ik}) = g(r_{ij})\, g(r_{ik})\, g(r_{jk}) \tag{5.11}$$

which is exact only in the HNC approximation.

The results for the liquid ^{4}He energy with Lennard-Jones potential,[5] and with g as given in HNC and HNC/4 approximations are shown in Table III. The difference $(W+U)_{HNC} - (W+U)_{HNC/4}$ is rather small while that between $E_{JF,HNC}$ and $E_{JF,HNC/4}$ is quite appreciable. The effective potentials V_{JF} and V are shown in Fig. 11 for $r<d$. The V_{JF} contains the singular v and is very large at small r making E_{JF} too sensitive to g at small r.

In lowest order ($g=f^2$) the W and E_{JF} are identical as can be seen by integrating the $(\nabla f)^2$ term by parts. Thus when $g=f^2$ the integral from the core region above the $V=\lambda_0$ line in Fig. 11 exactly cancels that from the dip below the line. When $g \neq f^2$ the cancellation is not exact. In principle for exact distribution functions $(W+U)$ must equal E_{JF}, so that

$$\frac{1}{2\Omega}\sum_{ij}\int g[V_{JF}(r) - V(r)]\, d^3r = U, \tag{5.12}$$

and it is obviously simpler to calculate $W+U$ directly when g is only approximately known. Even the $g_{HNC/4}$ is not accurate enough for use with the Jackson-Feenberg identity. The small difference between $(W+U)_{HNC}$ and $(W+U)_{HNC/4}$ may be used as representative of the error in the HNC/4 integral equation.

Figure 12 shows the variation of liquid ^{4}He energy at experimental density with d/r_0. When

TABLE III. The $E(\rho)$ for liquid ^{4}He with LJ potential in HNC and HNC/4 approximations. The E_{JF} is calculated with Jackson-Feenberg transformation, and $(W+U)$ is discussed in text.

$\rho\left(\frac{\text{Atoms}}{\sigma^3}\right)$	Energy (°K per atom) $(W+U)$ HNC	$(W+U)$ HNC/4	E_{JF} HNC	E_{JF} HNC/4
0.26	−5.452	−5.530	−5.027	−5.318
0.29	−5.703	−5.820	−5.045	−5.454
0.32	−5.819	−5.988	−4.885	−5.435
0.35	−5.778	−6.009	−4.493	−5.208
0.38	−5.554	−5.857	−3.835	−4.737
0.41	−5.125	−5.513	−2.879	−3.991

$d \approx 2r_0$ the energy is quite insensitive to d and hence most of our calculations are carried out with $d = 2r_0$. This range of f is still much shorter than that of the exponential f used in Monte Carlo calculations.[4,5] Details of other results on ^{4}He and comparisons are given in the last section.

VI. FERMI FLUID CALCULATIONS

The sum of direct $g(\vec{k}_m, \vec{k}_n)$ diagrams can be easily calculated with the integral equation (4.4). Let this sum be denoted by g_B, and let

$$h(r) = g_B/f^2 . \tag{6.1}$$

Figure 13 shows $g(\vec{k}_m, \vec{k}_n)$ diagrams in which only

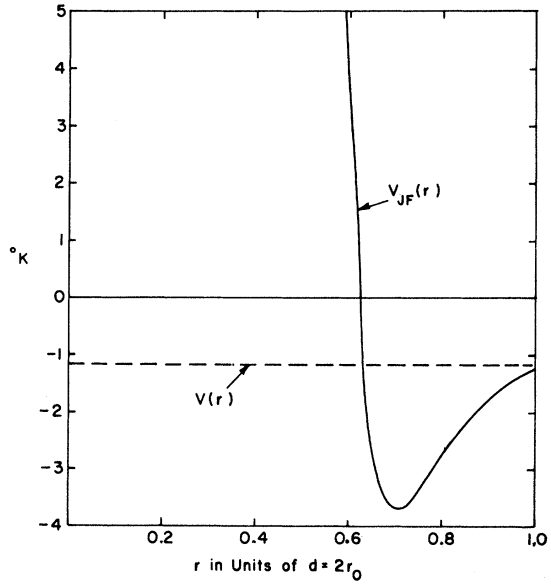

FIG. 11. The effective potentials in liquid ^{4}He at $\rho = 0.35$ Atoms/σ^3 and $d = 2r_0$ with LJ potential.

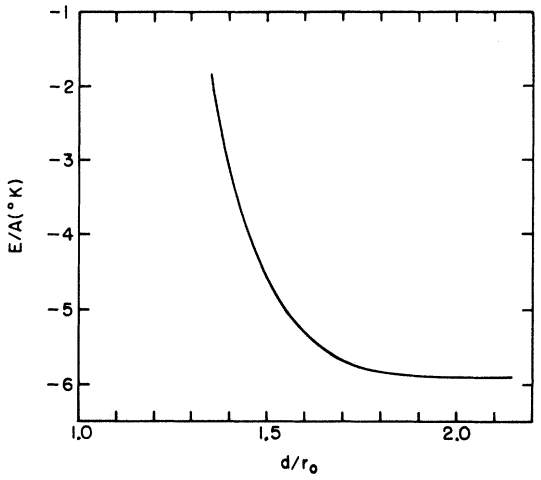

FIG. 12. Variation of energy with d in liquid ^{4}He at $\rho = 0.35$ Atoms/σ^3 with LJ potential.

the pair of particles in states $\vec{k}_m$ and $\vec{k}_n$ is exchanged. As discussed previously all HNC, or better HNC/4 chains connecting m and n must be summed to any number of particles. The effect of this sum is the multiplier h of Eq. (6.1), and it is denoted by a crossed line in diagram G.4. The contribution of G.4 is obviously

$$g_B(\vec{k}_m, \vec{k}_n)_{ex} = -e^{i(\vec{k}_m - \vec{k}_n)\cdot\vec{r}} g_B . \tag{6.2}$$

Sum over exchanges $\vec{k}_m, \vec{k}_n$ gives the square of the

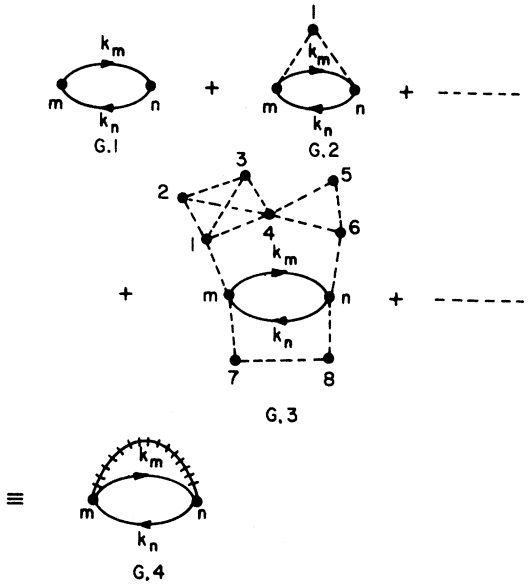

FIG. 13. Fermi $g(\vec{k}_m, \vec{k}_n)$ diagrams with one exchange.

Slater function

$$S(k_F r) = \frac{1}{N}\sum_i e^{i\vec{k}_i\cdot\vec{r}}\,,$$
$$= \frac{3}{k_F^3 r^3}[\sin(k_F r) - k_F r\cos(k_F r)]\,, \qquad (6.3)$$

[this S should not be confused with that of Eq. (4.1)], and the contribution to the Fermi radial distribution function (3.3) is

$$g_{B\text{ex}} = -S^2(k_F r) g_B\,. \qquad (6.4)$$

Exchange of a particle in state $\vec{k}_m$ or $\vec{k}_n$ with another particle gives diagrams of type H.1 in Fig. 14. The sum of all direct diagrams connecting m and 1 is represented by the double broken line and equals $[g_B(r_{m1}) - 1]$. The g_B includes a unit contribution from m and 1 unconnected, and this is subtracted to insure that only the irreducible diagrams are counted. A $S^2(k_F r_{1n})$ is obtained by summing the exchanges, addition of diagrams with and without F_{1n} gives f_{1n}^2 which is converted to g_{1n} by summing all direct diagrams connecting 1 and n. Thus the double full line $1n$ denotes

$$F_{\text{ex}}(r_{1n}) = \tfrac{1}{2} g_B(r_{1n}) S^2(k_F r_{1n})\,, \qquad (6.5)$$

where the factor $\frac{1}{2}$ comes from requiring that the spins of particles 1 and n be parallel. The contribution of these diagrams is

$$g_{\text{H.1}} = -2g_B\rho\int [g_B(r_{m1}) - 1] F_{\text{ex}}(r_{1n})\, d^3r_1$$
$$\equiv f^2 h_1\,. \qquad (6.6)$$

The factor 2 arises because m and n may be interchanged.

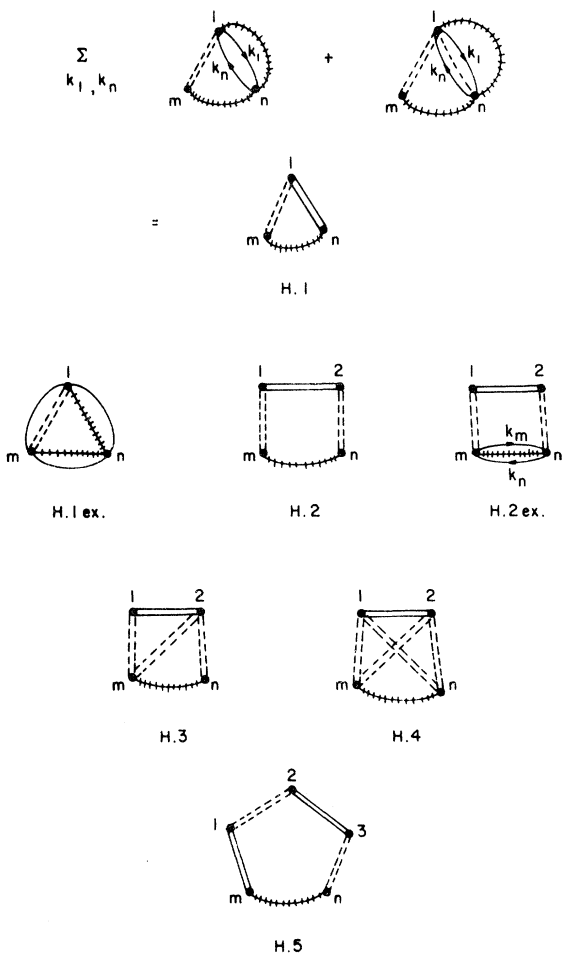

FIG. 14. Fermi g diagrams with exhanges in the chains.

Two successive exchanges between particles in states n and 1 and 1 and m give three-particle exchange diagrams. The sum of all three-particle exchange diagrams with any number of direct chains is represented by the diagram H.1ex in Fig. 14, and its contribution

$$g_{\text{H.1ex}} = S(k_F r) g_B\rho \int [g_B(r_{m1}) - 1] S(k_F r_{m1}) g_B(r_{n1}) S(k_F r_{n1})\, d^3r_1 \qquad (6.7)$$

cancels $g_{\text{H.1}}$ at small r when m and n have parallel spins.

In this notation, it is quite simple to write the contributions of more complicated exchange diagrams. That of H.2 in Fig. 14 is, for example,

$$g_{\text{H.2}} = -g_B\rho^2 \int [g_B(r_{m1}) - 1] F_{\text{ex}}(r_{12}) [g_B(r_{n2}) - 1]\, d^3r_1 d^3r_2 \equiv f^2 h_2\,. \qquad (6.8)$$

Figure 15 shows the functions $g_{2\text{-body}}$ ($=f^2$), Δg_{HNC} ($=g_B$ in HNC approximation $-f^2$), Δg (the difference between g_B in HNC and HNC/4 approximations), $g_{\text{H.1}}$, and $g_{\text{H.2}}$ in liquid ^{3}He at experimental equilibrium density. The F_{ex} is a rather small function because g is small where $S(k_F r)$ is unity and vice versa. Hence diagrams with exchanges in the chains give a small contribution. We neglect diagram H.4 because its contribution should be much smaller than Δg which itself is small. The maximum contributions of H.3 and H.5 are respectively 0.018 and 0.016 at $r \sim 0.6d$. More complicated exchange diagrams are expected to have still smaller contributions and are neglected. The g is given by

$$g = (g_B + g_{\text{H.2}})[1 - \tfrac{1}{2} S^2(k_F r)] + g_{\text{H.1}} + \tfrac{1}{2} g_{\text{H.1ex}} + g_{\text{H.3}} + \cdots\,. \qquad (6.9)$$

In the superposition approximation, the $g_3(\vec{r}_{ij}, \vec{r}_{ik})$ can be easily expressed in terms of the functions h and f^2 for various exchanges between particles i, j, and k.

The potential and the part of kinetic energy in which ∇^2 operates on a single f are given by expressions (5.7), (5.8), and (6.9). This contribution is denoted by W. The terms with ∇_1^2 operating on f_{12} and f_{13} give the term U as defined by Eq. (5.9) and calculated with Fermi three-particle distribution function containing exchange contributions.

Terms in which ∇_1^2 operates on φ_1 give the Fermi gas kinetic energy T,

$$T = \frac{\hbar^2}{2m} \tfrac{3}{5} k_F^2 . \tag{6.10}$$

The $\nabla_1 f_{12} \nabla_1 \varphi_{12}$ terms do not contribute to direct matrix elements when f is spherically symmetric. Its contribution through exchange of 1 and 2 is given by

$$W_F = \frac{\hbar^2}{m} \frac{1}{\Omega} \sum_{k_1, k_2} \int \frac{\nabla f}{f} \cdot i\vec{k}\, e^{i(\vec{k}_1 - \vec{k}_2)\cdot\vec{r}} (g_B + g_{H.2}) d^3r , \tag{6.11}$$

and that from the exchange of 1 and 3 is

$$U_F = \frac{\hbar^2}{m} \frac{1}{\Omega^2} \sum_{k_1 k_2 k_3} [g_B(r_{13}) + g_{H.2}(r_{13})][g_B(r_{23}) + g_{H.2}(r_{23})]$$
$$\times [g_B(r_{12}) + g_{H.2}(r_{12})]\, e^{i(\vec{k}_1 - \vec{k}_3)\cdot\vec{r}_{13}} \left(i\vec{k}_1 \cdot \frac{\nabla f_{12}}{f_{12}} \right) d^3r_{12}\, d^3r_{13} . \tag{6.12}$$

The total energy is

$$E = T + W + W_F + U + U_F . \tag{6.13}$$

The results of liquid ^{3}He calculations with Bose f having $d = 2r_0$ are given in Tables IV and V. These results are in very close agreement with those obtained by Monte Carlo calculations[4] within the Wu and Feenberg formalism.[15] When the present calculation is carried out with a spherically symmetric Bose f, its assumptions are identical to those of the Wu-Feenberg formalism, and only the computational method is different.

Calculations with the angle-dependent correlation functions obtained by solving Eqs. (2.13) and (2.14) can be simplified by defining a k- and l- dependent effective interaction $V^l(k, r)$,

$$V^l(k, r < d) = \lambda_0^l(k) ,$$
$$V^l(r > d) = v^l . \tag{6.14}$$

When $d = 2r_0$, the lowest-order two-body contribution with these f's,

$$(W + W_F)_{\text{L.O.}} = \frac{1}{2\Omega^2} \sum_{ij} \langle \varphi_i \varphi_j - S_{\uparrow\uparrow} \varphi_j \varphi_i | [\sum_l f^{l2}(k, r) V^l(k) P_{ij}^l] | \varphi_i \varphi_j \rangle \tag{6.15}$$

is ~10% lower (algebraically) than that with the Bose f (Table IV).

The higher-order contribution (from more than two-body clusters) is only ~25% of the lowest-order contribution, and it is calculated with the average f as defined in Sec. II. This average f is very similar to the Bose f and hence higher-order contributions are almost identical in the two calculations (Table IV).

The U and U_F are both higher-order terms not involving v^l, and they can be easily calculated with the average f and the functions h. However, particularly in neutron matter, the evaluation of higher-order contributions to $W + W_F$ is nontrivial even when a single average f is assumed because of the l dependence of the two-body interaction. The effect of the many-body system is to push the two interacting particles closer, and we assume that this effect is spherically symmetric. The $(W + W_F)$ including higher-order contributions is then given by

$$(W + W_F) = \frac{1}{2\Omega^2} \sum_{ij} \{ \langle \varphi_i \varphi_j | [\sum_l f^{l2}(k, r) V^l(k) P_{ij}^l](h + h_1 + h_2) | \varphi_i \varphi_j \rangle$$
$$- \delta_{\uparrow\uparrow} \langle \varphi_j \varphi_i | [\sum_l f^{l2}(k, r) V^l(k) P_{ij}^l](h + h_2) | \varphi_i \varphi_j \rangle + \delta_{\uparrow\uparrow} \langle \varphi_i \varphi_j | [\sum_l f^{l2}(k, r) V^l(k) P_{ij}^l] h_{\text{1ex}} | \varphi_i \varphi_j \rangle \} . \tag{6.16}$$

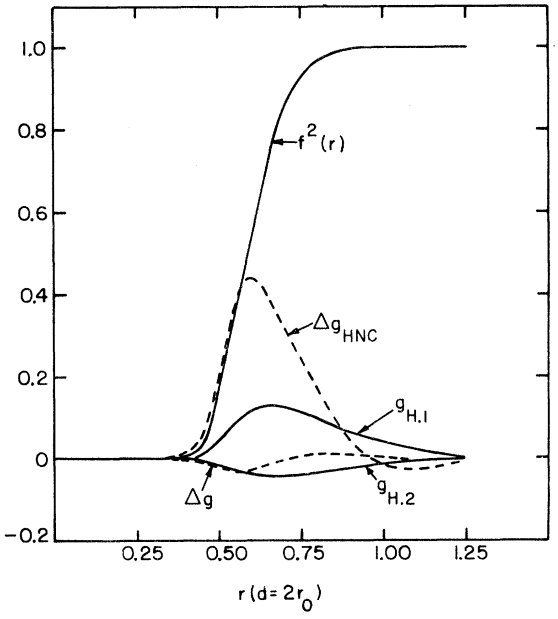

FIG. 15. Contributions to the radial distribution function in liquid ^{3}He at $\rho = 0.277$ Atoms/σ^3, $d = 2r_0$, with LJ potential. Distance r in units of d.

Here h_{1ex} and h_2 represent the contributions of diagrams H.1$_{ex}$ and H.2. The above expression is correct in lowest order, and the errors in higher orders involve only the differences between V^l or f^l. Table VI gives the contributions to the energy of neutron matter with Reid potential for $d = 2r_0$. The error due to the approximate treatment of the state dependence of n-n interaction should be a few percent of the $\Delta(W + W_F)_{H.O.}$ contribution. The numerical methods and errors involved therein are discussed in the Appendix.

Recently Miller *et al.*[16] have suggested that the Hamiltonian for neutron matter could be written

TABLE IV. The contributions to $E(\rho)$ of liquid ^{3}He with LJ potential in HNC/4 approximation, with the mass-3 Bose$f$, and state-dependent correlation functions (S.D.f). The sum of all higher-order contributions is simply E-T-$(W + W_F)_{L.O.}$.

		Energy per atom (°K)			
		$(W + W_F)_{L.O.}$ (°K)		All H.O. (°K)	
ρ (Atoms/σ^3)	T	Bose f	S.D.f	Bose f	S.D.f
0.187	2.31	−4.01	−4.47	0.49	0.44
0.217	2.56	−4.68	−5.18	0.79	0.72
0.247	2.79	−5.34	−5.88	1.19	1.10
0.277	3.01	−6.00	−6.58	1.72	1.62
0.307	3.22	−6.68	−7.26	2.41	2.28
0.337	3.43	−7.33	−7.94	3.23	3.12

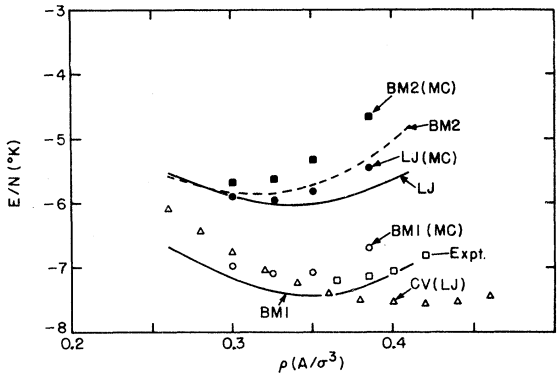

FIG. 16. The $E(\rho)$ for liquid ^{4}He. The full and broken lines give the results of present calculations with LJ, BM1, and BM2 potentials (Ref. 5). The full squares, circles, and hollow circles, respectively, give the results of Monte Carlo calculations with exponential f, and BM2, LJ, and BM1 potentials (Ref. 5). The experimental data (Ref. 5) and results of constrained variational calculations (Ref. 6) are shown by hollow squares and triangles.

as

$$H = \frac{-\hbar^2}{2m}\sum_i \nabla_i^2 + \sum_{i<j} \bar{v}_{ij} + \sum_{i<j}\left(\sum_l v_{ij}^l P^l - \bar{v}_{ij}\right), \tag{6.17}$$

where $\bar{v}_{ij}$ is a state independent interaction. They define

$$\bar{v}_{ij} = \sum_l C_l\, v_{ij}^l \tag{6.18}$$

and choose C_l such that the last term of Hamiltonian [Eq. (6.17)] gives zero contribution in lowest order. Its higher-order contributions are neglected and approximate Wu-Feenberg calculations are carried out for the first two terms of [Eq. (6.17)]. Thus, in effect, the state dependence of v_{ij} is treated correctly only in lowest order.

TABLE V. The $E(\rho)$ of liquid ^{3}He with LJ potential. The four columns list the results for mass-3 Bose fluid, Fermi ^{3}He energy with the f for Bose fluid, then with state-dependent f in HNC/4 approximation, and finally the S.D.f energy in HNC approximation.

	Energy/atom (°K)			
ρ (Atoms/σ^3)	HNC/4 mass-3 Bose	HNC/4 Bose$f$	HNC/4 S.D.f	HNC S.D.f
0.187	−2.78	−1.21	−1.72	−1.70
0.217	−2.95	−1.33	−1.91	−1.86
0.247	−3.01	−1.35	−1.99	−1.91
0.277	−2.92	−1.27	−1.95	−1.82
0.307	−2.66	−1.05	−1.75	−1.58
0.337	−2.22	−0.67	−1.39	−1.16

TABLE VI. The contributions to $E(\rho)$ of neutron gas with Reid potential in HNC/4 approximation. $\Delta(W+W_F)$ is the higher-order contribution to $W+W_F$.

ρ (N/fm^3)	Contributions to energy (MeV/neutron) T	$(W+W_F)_{\text{L.O.}}$	$\Delta(W+W_F)$	U	U_F	All H.O.	E
0.2	40.7	−21.4	−0.6	0.6	0.5	0.5	19.77
0.6	84.6	−26.4	+0.6	11.3	6.9	18.7	77.00
1.0	119.0	−11.0	16.3	30.8	14.6	61.8	169.7
1.4	149.0	21.9	44.5	54.5	22.4	121.0	292.0
1.8	176.0	70.6	82.5	79.8	29.9	192.0	438.8
2.2	201.0	133.0	129.0	106.0	37.3	272.0	606.8
2.6	225.0	209.0	182.0	133.0	44.6	359.0	793.4
3.0	248.0	296.0	241.0	160.0	51.8	453.0	997.4
3.4	269.0	394.0	307.0	189.0	59.0	554.0	1217.4
3.8	290.0	502.0	378.0	216.0	66.2	661.0	1452.4
4.2	310.0	618.0	456.0	246.0	73.5	773.0	1701.6
4.6	329.0	743.0	538.0	273.0	80.8	892.0	1963.4
5.0	348.0	875.0	625.0	300.0	89.9	1015.0	2237.6

The energies obtained by Miller *et al.* are up to 30% higher than those with the constrained variation method for $k_F < 2.5$ fm^{-1} ($\rho \simeq 0.53$ fm^{-3}). The maximum density in their calculations is $k_F = 3.5$ fm^{-1} or $\rho = 1.4$ fm^{-3}, and their energy for it is approximately half of that given by constrained variation. They discuss improvements in their calculations with $\bar{v}_{ij}$ which may decrease the difference.

Two comments on the separation of the Hamiltonian [Eq. (6.17)] may be appropriate here. When the interacting particles are very close the interaction must be mostly in relative S state, irrespective of the order of the contribution. However, for an average of v^l of type (6.18) the higher-order contributions to the interaction at small r will involve the potentials in high-l states. This difficulty is partly avoided in the approximation (6.16). Secondly, the partial lowest-order contribution is very sensitive to the range of f (see Sec. VII for more details) while the total energy is not. This may introduce a significant uncertainty in the parameters C_l.

The smallness of the difference between energies calculated in HNC and HNC/4 approximations (Table V for ^{3}He, and Table VII for n gas) indicates that all relevant direct diagrams have been summed by HNC/4 integral equation. The energy change on inclusion of complicated exchange diagrams like H.3 and H.5 of Fig. 14 is less than half of $E_{\text{HNC/4}} - E_{\text{HNC}}$ and justifies the truncation of the exchange diagram sum.

TABLE VII. The $E(\rho)$ of n gas with Reid potential in HNC, and HNC/4 approximations.

ρ (n/fm^3)	E/n (MeV) HNC	HNC/4
0.2	19.77	19.77
0.6	77.08	77.00
1.0	170.5	169.7
1.4	293.5	292.0
1.8	440.4	438.8
2.2	607.3	606.8
2.6	790.5	793.4
3.0	987.9	997.4
3.4	1197.5	1217.4
3.8	1417.8	1452.4
4.2	1647.3	1701.6
4.6	1885.3	1963.4
5.0	2130.6	2237.6

VII. CONCLUSIONS

Results of the constrained variational calculation in lowest order and of accurate energy cal-

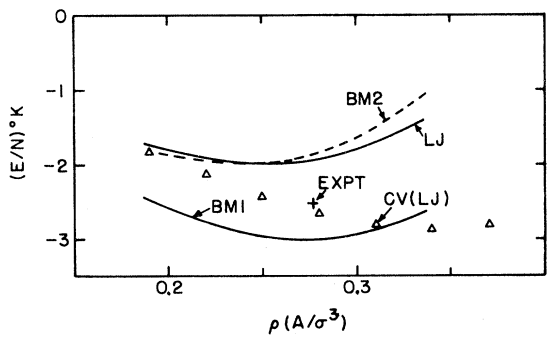

FIG. 17. The $E(\rho)$ for liquid ^{3}He (see caption of Fig. 16 for notation). The + shows experimental ground-state data.

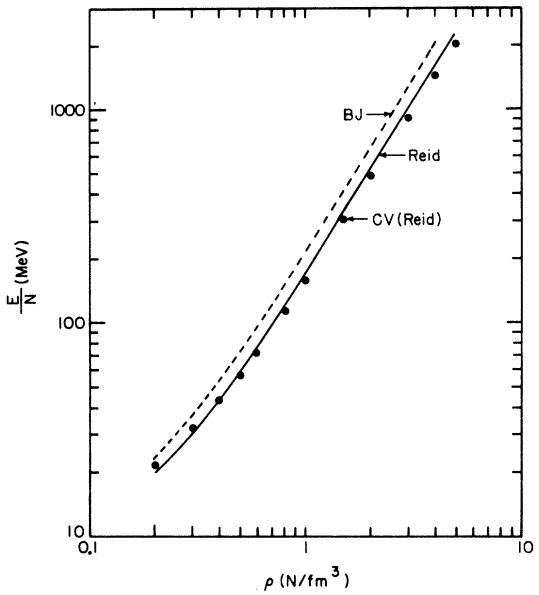

FIG. 18. The $E(\rho)$ for n gas. The full and broken lines give the results with Reid, and the modified Reid potential, and the points show results of lowest-order constrained variation (Ref. 6) with Reid potential.

culations with unconstrained d are compared in Figs. 16–18. The two calculations agree very well in neutron matter (Fig. 18), whereas the simple lowest-order calculation overestimates the binding energies and equilibrium densities of liquid ^{3}He and ^{4}He by ~25% relative to the other (Table VIII).

The results of Monte Carlo calculations in ^{4}He

TABLE VIII. The ground-state properties of liquid ^{3}He and ^{4}He, with LJ, BM1, and BM2 potentials. The parameters of the potentials are given in Ref. 5. The (CV) labels result with lowest-order constrained variation (Ref. 6). Compressibility K in percent per atmosphere.

	$\rho_0(\sigma^{-3})$	E/N (°K)	K (%/atm)
	^{3}He		
Experimental	0.277	−2.52	3.5-3.8
LJ (CV)	0.342	−2.87	2.56
LJ	0.256	−1.99	3.86
BM1	0.276	−3.02	2.73
BM2	0.245	−1.98	3.88
	^{4}He		
Experimental	0.365	−7.2	1.02
LJ (CV)	0.425	−7.58	1.13
LJ	0.344	−6.01	1.31
BM1	0.349	−7.43	1.11
BM2	0.317	−5.86	1.62

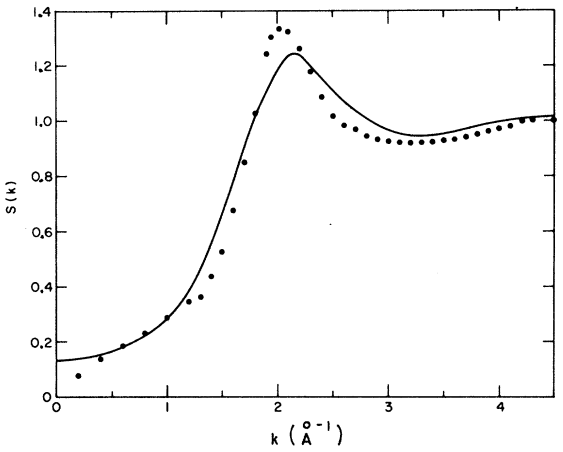

FIG. 19. The $S(k)$ in ^{4}He liquid at $\rho = 0.365$ Atoms/σ^3. The points show experimental data (Ref. 17), and the full line gives results of calculations with BM2 potential.

with exponential $[f = \exp(\alpha/r^5)]$ correlation functions[5] are also shown in Fig. 16. At higher densities our calculations give slightly lower energies; however, the difference for LJ potential is comparable to $(E_{\mathrm{HNC}} - E_{\mathrm{HNC}/4})$ and hence should not be taken too seriously. The exponential f should be reasonable for LJ potential because the solution of Eq. (2.5) has this form at small r with LJ $v(r)$. There is no physical reason why this exponential f should describe correlations with the Bruch-McGee potentials, and the present f indeed seem to give significantly lower energies with

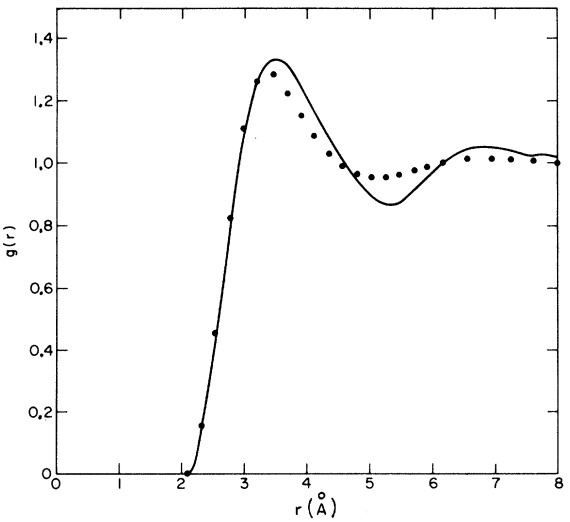

FIG. 20. The $g(r)$ in ^{4}He liquid at $\rho = 0.365$ Atoms/σ^3. The full line is from Achter and Meyer's (Ref. 17) analysis of experimental $S(k)$, and the points are calculated with BM2 potential.

BM1 and BM2 potentials. The equilibrium properties are given in Table VIII, and BM1 potential appears to yield a remarkably close description. The authors (Bruch and McGee[17]), however, point out that the BM2 potential gives the best fit to dilute gas properties. The radial distribution function $g(r)$, and its Fourier transform, the liquid structure factor $S(k)$ as computed with BM2 potential are compared with the experimental analysis of Achter and Meyer[18] in Figs. 19 and 20. The differences in $g(r)$ and $S(k)$ as calculated from LJ, BM1, and BM2 potentials are smaller than that between the experimental and calculated.

The distribution functions as calculated from integral equations have been criticized as inaccurate[5] or unreliable[19] for energy calculations. The decent convergence as well as the close agreement with Monte Carlo calculations obtained here with integral equations can be attributed to the following. First, HNC/4 is a better integral equation than HNC or PY used in Ref. 5. Second, the present method of calculating energies from an approximate $g(r)$ is less sensitive to the errors in $g(r)$ than the Jackson-Feenberg method used in Refs. 5 and 19. Third, the effective potential V is small with the present choice of f. With the exponential correlation functions used in Ref. 5, the V_{JF} goes to $+\infty$, while V goes to $-\infty$, making E too sensitive to g at small r. The range of our $f(\sim 2r_0)$ is also smaller than for the exponential f, and the magnitude of higher-order cluster contributions is smaller.

Previous best variational calculations gave a minimum at -1.35°K[4] for ^{3}He with LJ potential and spherically symmetric f. We obtain the same result with Bose f (Table V). The much lower energies in Fig. 17 are a direct consequence of allowing angular variation and state dependence in the correlation function. In the present work, this dependence is averaged over in the calculation of many-(>2) body clusters, and hence we can only conclude that energy gains of the order of 0.6°K may be obtained by allowing state dependence in correlation functions. The BM1 and BM2 potentials, respectively, overbind and underbind ^{3}He liquid.

TABLE IX. The contributions to $E(\rho)$ of neutron gas with Reid potential in HNC/4 approximation for various values of d/r_0.

ρ (N/fm^3)	(E/N) (MeV)	$d/r_0=1.2$	1.6	2.0
1.0	Total	204.4	177.3	169.7
	L.O.	156.3	123.7	108.0
	H.O.	38.1	53.6	61.7
3.0	Total	1174.0	1037.7	997.4
	L.O.	982.5	710.6	544.3
	H.O.	191.5	327.1	453.1
5.0	Total	2467.7	2266.0	2237.6
	L.O.	2117.5	1595.0	1223.0
	H.O.	350.2	671.0	1014.6

Table IX shows the total energy, the lowest-order, and higher-order contributions to it for the neutron gas at $d/r_0=1.2$, 1.6, and 2.0. The total energy is much less sensitive to d than its decomposition into lowest and higher cluster contributions. The higher-order contributions increase by a factor of 1.5–3 whereas the total energy decreases only by 10–15% as d is increased from 1.2 to $2r_0$.

The value of d is $\sim 1.2r_0$ in constrained variational calculations. Thus correlations with $d=1.2r_0$ are mainly two-body correlations because on the average there is only one neutron within the correlation volume of any. The small higher-order cluster contributions at $d=1.2r_0$ come from events in which two (or more) neutrons come within the correlation volume of a neutron. In lowest-order calculations, these are neglected assuming that they cancel events in which the neutron can have larger correlation volume because there is nothing within $1.2r_0$ from it. It is remarkable how well the lowest order for $d=1.2r_0$ agrees with the total energy for $d=2r_0$.

A product of two-body correlation functions is, of course, only an approximate way to express correlations in events in which many (>2) particles are simultaneously correlated. Hence the result of our accurate energy calculation can at best be interpreted as an upper bound. Effects of introducing an explicit three-body correlation in liquid ^{4}He have been estimated by Davison[20] with the correlated basis perturbation theory[14] to be ~ -0.76°K. Thus the total estimated energy of ^{4}He with LJ potential is -6.76°K, which agrees very well with -6.63°K as estimated by Kalos[21] from a direct solution of a 32-body Schrödinger equation plus corrections for finite N. This energy is also closer to the -7.58°K given by constrained variation (CV).

In conclusion, we find that the CV method is fairly accurate for dense systems like neutron gas interacting via a soft-core potential. In liquid He, it overestimates the binding energies because the events in which two or more atoms come within the correlation volume of an atom give a substantial repulsive contribution. The estimate of this contribution with a product wave function could be as much as twice the true value.

We should like to thank Mikkel Johnson and

Baird Brandow for interesting discussions. One of us (V.R.P.) also wishes to thank the Cornell Laboratory of Nuclear Studies for its hospitality.

APPENDIX: NUMERICAL METHODS

The contribution of diagram E.9 of Fig. 8

$$\hat{S}_{mn} = \tfrac{1}{2}\rho^2 \int F_{m1} F_{n1} F_{12} F_{m2} F_{n2} d^3r_1 d^3r_2 , \qquad \text{(A1)}$$

can be trivially written as

$$\hat{S}_{mn} = \pi\rho^2 \int F_{m1} F_{m2} r_{m1}{}^2 r_{m2}{}^2 dr_{m1} dr_{m2} \times \sin\theta_{m1} F_{n1} d\theta_{m1} \sin\theta_{m2} F_{n2} d\theta_{n2} F_{12} d\varphi_{12} \qquad \text{(A2)}$$

by choosing $\hat{\mathbf{r}}_{mn}$ as the Z axis, and

$$\varphi_{12} = \varphi_{m2} - \varphi_{m1} . \qquad \text{(A3)}$$

For chosen values of r_{m1}, r_{m2}, θ_{m1}, θ_{m2}, the φ_{12} integration is independent of r_{mn} and hence it is very economical to evaluate $S(r_{mn})$ simultaneously for various values of r_{mn}. The integral is zero for $r > 2d$ and was evaluated at 20 points between 0 and $2d$.

The integral equation (4.4) is highly nonlinear, and it is very desirable to have a good initial input for solving it by iteration. All the calculations were initiated at rather small densities (~0.15 Atom/σ^3 in liquid He) where it is simpler to solve it with $g = f^2$ as the initial input. The density is gradually increased in steps of ~10%, and the consistent $g(r)$ of the previous density is scaled with respect to r_0 and used as the initial input. The standard averaging over input-output solutions is used to improve the convergence.

In Fermi systems Eq. (2.13) is solved for $l = 0$, 1, and 2 at seven values of k. The $f(l, k)$ for higher values of l is approximated with the $f(1, k)$ and $f(2, k)$. The over-all numerical accuracy of the presented results is estimated to be ~2% of $(W + W_F)$, or ~0.1°K in liquid helium.

---

*Work supported in part by the National Science Foundation.

†On study leave from the Tata Institute of Fundamental Research, Bombay-5, India.

[1]H. A. Bethe, in Proceedings of the International Astronomical Union Symposium on Physics of Dense Matter, Boulder, Colorado, 1972 (to be published).

[2]P. J. Siemens and V. R. Pandharipande, Nucl. Phys. A173, 561 (1971).

[3]G. Baym, C. Pethick, and P. Sutherland, Astrophys. J. 170, 299 (1971).

[4]D. Schiff and L. Verlet, Phys. Rev. 160, 208 (1967).

[5]R. D. Murphy and R. O. Watts, J. of Low Temp. Phys. 2, 507 (1970).

[6]V. R. Pandharipande, Nucl. Phys. A178, 123 (1971).

[7]V. R. Pandharipande, Nucl. Phys. A181, 33 (1972).

[8]V. R. Pandharipande and V. K. Garde, Phys. Letters 39B, 608 (1972).

[9]R. V. Reid, Ann. Phys. (N.Y.) 50, 411 (1968).

[10]L. H. Nosanow, Phys. Rev. 146, 120 (1966).

[11]M. Gaudin, J. Gillespie, and G. Ripka, Nucl. Phys. A176, 237 (1971).

[12]J. M. J. van Leeuwen, J. Groeneveld, and J. de Boer, Physica 25, 792 (1959).

[13]E. Feenberg, *Theory of Quantum Fluids* (Academic, New York, 1969).

[14]H. W. Jackson and E. Feenberg, Ann. Phys. (N.Y.) 15, 266 (1961).

[15]F. Y. Wu and E. Feenberg, Phys. Rev. 128, 943 (1962).

[16]M. Miller, C. W. Woo, J. W. Clark, and W. J. Ter Louw, Nucl. Phys. 184, 1 (1972).

[17]L. W. Bruch and I. J. McGee, J. Chem. Phys. 52, 5884 (1970).

[18]E. K. Achter and L. Meyer, Phys. Rev. 188, 291 (1969).

[19]Hing-Tat Tan and E. Feenberg, Phys. Rev. 176, 370 (1968).

[20]T. B. Davison, Ph.D. thesis, Washington University, 1968 (unpublished).

[21]M. H. Kalos, Phys. Rev. A 2, 250 (1970.